Sources and sinks of dissolved inorganic carbon in an urban tropical coastal bay revealed by δ13C-DIC signals

Luiz Cotovicz, Bastiaan Knoppers, Loris Deirmendjian, Gwenaël Abril

Sources and sinks of dissolved inorganic carbon in an urban tropical coastal bay revealed by δ^{13}C-DIC signals

Luiz C. Cotovicz Jr.[*a,b]; Bastiaan A. Knoppers[a]; Loris Deirmendjian[b]; Gwenaël Abril[a,b,c]

[a] Programa de Geoquímica, Universidade Federal Fluminense, Niterói, RJ, Brazil

[b]Laboratoire, Environnements et Paléoenvironnements Océaniques et Continentaux (EPOC) UMR 5805, CNRS – Université de Bordeaux – Pessac, France

[c] Biologie des Organismes et Ecosystèmes Aquatiques (BOREA), UMR 7208, Muséum National d'Histoire Naturelle, CNRS, SU, UCN, UA, IRD, 61 rue Buffon, 75231, Paris cedex 05, France.

* Corresponding author: lccjunior@id.uff.br

Abstract

Dissolved inorganic carbon (DIC), its stable isotope composition (δ^{13}C-DIC) and ancillary parameters of the water column were investigated in a eutrophic tropical marine-dominated estuary surrounded by a large urban area (Guanabara Bay, Rio de Janeiro, Brazil). Most negative δ^{13}C-DIC signatures (down to -6.1‰) were found in polluted regions affected by direct sewage discharges where net heterotrophy induces high partial pressure of CO_2 (pCO_2) and DIC concentrations. Keeling plot was applied to this polluted region and determined the δ^{13}C-DIC sewage signature source of -12.2‰, which is very consistent with isotopic signature found in wastewater treatment plans. These negative δ^{13}C-DIC signatures (i.e., DIC depleted in ^{13}C) were restricted to the vicinity of urban outlets, whereas in the largest area of the bay δ^{13}C-DIC signatures were more positive (i.e., DIC enriched in ^{13}C). The most positive δ^{13}C-DIC signatures (up to 4.6‰) were found in surface waters dominated by large phytoplankton blooms, with positive correlation with chlorophyll *a* (Chl *a*). In the largest area of the bay, the preferential uptake of the lighter stable carbon isotope (^{12}C) during photosynthesis followed the Rayleigh distillation, and appeared as the most important driver of δ^{13}C-DIC variations. This reveals an important isotopic fractionation (ε) by phytoplankton due to successive algal blooms that has turned the remaining DIC pool enriched with the heavier stable carbon isotope (^{13}C). The calculated diel apparent ε showed higher values in the morning (18.7‰ to 21.6‰) and decreasing in the afternoon (6.8‰ to 11.1‰). ε was positively correlated to the pCO_2 ($R^2 = 0.88$, $p = 0.005$) and DIC concentrations ($R^2 = 0.73$, $p = 0.02$), suggesting a decline in carbon assimilation efficiency and decreasing uptake of the lighter carbon under CO_2 limiting conditions. The eutrophic coastal waters of Guanabara Bay have δ^{13}C-DIC signatures well above that found in estuaries, shelf and ocean waters worldwide.

Keywords: δ^{13}C-DIC signatures; coastal eutrophication; carbon cycling; Guanabara Bay

1. Introduction

The coastal zone is one of the most biologically active areas of the biosphere, and plays an important role in the global carbon cycle (Gattuso et al. 1998). Estuaries are considered prominent coastal environments, which receive large amounts of organic matter from land, and exchange material with the adjacent ocean and the atmosphere (Borges and Abril, 2011; Chen et al. 2013). The most recent global estimation of estuarine CO_2 emissions to the atmosphere is about 0.1 Pg C yr^{-1} (Chen et al. 2013). These emissions occur because in estuaries the consumption of organic carbon exceeds net primary production, and the net heterotrophy in the ecosystem leads to high pCO_2 levels (Gazeau et al. 2004; Borges and Abril, 2011), together with lateral CO_2 inputs from tidal wetlands (Cai and Wang 1998., Bouillon et al. 2003; Bouillon et al. 2011) and rivers (Frankignoulle et al. 1998; Hunt et al. 2011; Joesoef et al. 2017). However, it must be highlighted that the high diversity of estuarine morphological types and associated ecosystems creates strong local and regional differences that hinders the extrapolation of results for global estimations, which remain uncertain (Borges, 2005).

The δ^{13}C-DIC is a helpful tool understanding biogeochemical cycling and tracing the sources, sinks and transformations of carbon in aquatic ecosystems (Gillikin et al. 2006; Burt et al. 2016). During photosynthesis, plants use preferentially the lighter stable carbon isotope (^{12}C) than the heavier stable carbon isotope (^{13}C). This carbon stable isotope discrimination leads to an isotopic fractionation and, thus, organic carbon in marine plants and algae are depleted in ^{13}C relative to their DIC source (Burkhardt et al. 1999). Therefore, aquatic primary production tends to leave the water rich in ^{13}C, increasing δ^{13}C-DIC signatures (Zeebe and Wolf-Gladrow, 2001). On the other hand, the degradation of organic carbon by respiring heterotrophic organisms, either in pelagic or in benthic compartments, produces CO_2 with approximately the same isotopic signature of the respired organic matter, decreasing δ^{13}C-DIC signatures (Kendall and Doctor, 2004; Miyajima et al. 2009; Bouillon et al. 2011; Bhavya et al. 2018).

The freshwater δ^{13}C-DIC endmember in estuaries could present very different values, and related to distinct isotopic signatures from the major sources and sinks, including biogenic and lithological sources, air-water CO_2 exchanges, and *in situ* metabolism (Mook and Tan, 1991; Campeau et al. 2017). This large heterogeneity leads to freshwater end-members generally ranging between -5‰ and -25‰, depending on the intensity of the different δ^{13}C-DIC sources and sinks (Kendall and Doctor, 2004; Finlay and Kendall, 2007). This results in marked changes in the stable isotope carbon composition across estuarine salinity gradients from freshwater to the sea (Fry, 2002). Very negative δ^{13}C-DIC signatures (down to – 20‰ or range), which shows a strong depletion of ^{13}C in the DIC pool, were documented in several estuaries, especially at low salinity regions, which are usually highly heterotrophic (Bouillon et al. 2007; Bouillon et al. 2011). Contrary to low salinity regions, the marine-dominated regions of estuaries exhibit higher δ^{13}C-DIC signatures that are usually in the range of -2‰ to +2‰ (mean approaching 0‰) due to a predominance of marine DIC and a limited influence of DIC from terrestrial sources (Mook and Tan, 1991; Chanton and Lewis, 1999; Gruber et al. 1999). Generally, the stable isotope signature of DIC in estuaries follows mixing process between marine and freshwater end-members (Mook and Tan, 1991), attesting that DIC levels are mainly controlled by physical processes (Wang et al. 2016). However, deviation from mixing curves are frequently reported (Coffin and Cifuentes, 1999; Bouillon et al. 2003; Gillikin et al. 2006; Miyajima et al. 2009; Bouillon et al. 2011; Bhavya et al. 2018). The δ^{13}C-DIC data below conservative mixing suggest prevalence of respiration that adds depleted δ^{13}C-DIC (Bouillon et al. 2003; Bouillon et al. 2011). On the other hand, in estuaries with important levels of photosynthesis, deviation above to the mixing curve can occur due to the

preferential uptake of the lighter stable carbon isotope (Coffin and Cifuentes, 1999; Zeebe and Wolf-Gladrow, 2001; Gillikin et al. 2006). In addition to the metabolic controls (respiration and photosynthesis), the δ^{13}C-DIC dynamic is also affected by physical controls such as the CO_2 exchange with the atmosphere and dissolution/precipitation of carbonate minerals (Finlay and Kendall, 2007). It is important to point out that when DIC reaches the equilibrium with atmospheric CO_2 concentrations, the δ^{13}C-DIC becomes close to the value of 0‰ (Bouillon et al. 2011). However, there is an important temperature-dependent equilibrium isotope fractionation of δ^{13}C-DIC (Zhang et al. 1995), and this can causes regional deviations from 0‰ depending on aquatic and atmospheric temperatures.

In addition to the high natural variability of δ^{13}C-DIC values in estuaries and coastal zones, the isotopic signature of the DIC can change in response to anthropogenic forcing (Finlay and Kendall, 2007; Yang et al. 2018). Human activities, such as land-use changes, wastewater discharges, and wetlands destruction, are altering carbon sources, sinks, cycling and budgets (Bauer et al. 2013). Although the use of δ^{13}C-DIC is well established for investigations of ecosystem metabolism and water mixing processes in estuaries, this parameter has been rarely used to describe the occurrence of anthropogenic perturbations such as eutrophication. In the tropics, the development of coastal megacities with inefficient treatment of wastewaters, combined with enhanced biological activity due to specific climatic features, leads to drastic modifications of the regional carbon cycle (Carreira et al. 2002; Cotovicz et al. 2015), which should impact the isotopic signature of the DIC. Here, we present the first measurements of δ^{13}C-DIC in a tropical coastal embayment that receives large amounts of untreated wastewaters from surrounding urban areas, which hosts a population of about 9 millions of inhabitants. Large inputs of domestic effluents into the bay enhanced the levels of aquatic primary production (Rebello et al. 1988), and turned the bay into a marked sink of CO_2 (Cotovicz et al. 2015). We hypothesized that these human perturbations of the estuarine system will have important impacts on the isotopic signature of the DIC that need a detailed characterization. We also expected uncommon isotopic signatures of these coastal waters compared to other estuarine and marine environments.

2. Materials and Methods

2.1. Study Area

Guanabara Bay (22°41–22°58 S and 43°02–43°18 W) is a tropical coastal embayment located at the SE-Brazilian coast (Fig. 1). The surface area is 384 km^2, the mean depth is 5.7 m, and the water volume is about 1870 x 10^6 m^3. The bay has a microtidal regime, and is a partially mixed estuary (Kjerfve et al. 1997), but under conditions of high solar incidence and high freshwater discharge the bay could present a strong vertical thermohaline stratification (Cotovicz et al. 2015). The annual freshwater inputs by the rivers is only about 100 m^3 s^{-1} (Kjerfve et al. 1997). The large difference between the high water volume and the low amount of freshwater inputs are reflected in high salinities along the Bay (averaging 29.5 ± 4.8), with few lower values (down to 15) at the vicinity of the small river mouths. Considering the bay as a whole, more than 85% of the water volume corresponds to seawater, whereas only 15% is attributed to freshwaters (Costa-Santos, 2015). The average time necessary to renew 50% of the total water volume with the tidal movements is 11.4 days, but with significant spatial differences, especially at the most confined regions (Kjerfve et al. 1997). Guanabara Bay is located in the intertropical zone, and the climate is characterized by a warm and wet summer, and a cooler and drier winter (Bidone and Lacerda,

2004). The annual freshwater input to the bay is approximately 100 ± 59 m^3 s^{-1}, and modest compared to the bay's water volume, which contributed to the predominance of polyhaline to euhaline waters. The bay is one of the most polluted coastal systems in the world that receives large inputs of untreated domestic and industrial effluents at approximately 25 m^3 s^{-1} (Kjerfve et al. 1997; Bidone and Lacerda, 2004). We compartmentalized the bay into five domains (sectors 1, 2, 3, 4, and 5) as described by Cotovicz et al. (2015; 2018a) for the treatment, computations and interpretation of the data (Fig. 1).

2.2. Experimental Design, Sampling Procedures and Laboratory Analysis

In 2013 and 2014, nine sampling campaigns were conducted for the analysis of δ^{13}C-DIC and ancillary parameters of the water column in Guanabara Bay. The water parameters were sampled in continuous on-line and/or discrete procedures. Continuous measurements were performed to analyze the water temperature, salinity, DO and pCO_2, as described by Cotovicz et al. (2015). Briefly, one submersible water pump was positioned at the side of the boat (depth of 0.5 m), providing continuous water flow to a measurement system located inside the boat. The continuous measurements of pCO_2 followed the equilibration technique using a marble-type equilibrator coupled to a non-dispersive infrared gas detector (LICOR 820) (Frankignoulle et al. 2001; Cotovicz et al. 2016a). The equilibrator had a response time lower than 4 minutes, and, as the boat speed during measurements was about 6 km h^{-1}, pCO_2 measurements were averaged over approximately 300m of the boat's track. One calibrated YSI 6600 V2 multiparameter probe measured continuously the water temperature, salinity and DO.

Discrete water samples were taken for δ^{13}C-DIC, chlorophyll *a* (Chl *a*), pheo-pigments, total alkalinity (TA), and dissolved inorganic phosphorus (PO_4^{3-}), accounting to about 16-19 stations distributed across the bay, except in December 2013, when only 8 stations could be sampled. Sub-surface water samples were collected at 0.5 m depth with a Niskin bottle, and conditioned (i.e. fixed and/or kept on ice in the dark) for further chemical analysis at the laboratory. The comparison between surface and bottom waters in terms of δ^{13}C-DIC concentrations and other physico-chemical parameters were performed at some stations, during the summer period, and during conditions of maximal vertical stratification at summer period in sectors 3, 4, and 5 (Cotovicz et al. 2016b).

The water was filtered with whatman GF/F glass-fibre filters (porosity 0.45 μm) followed by determination of suspended particulate material (SPM), Chl *a* and pheo-pigments. The filters were pre-combusted (at 500° C during 6 hours) and pre-weighted before utilization. After filtration, filters were dried in an oven at 50°C and then weighed. SPM was determined gravimetrically. Chl *a* and pheo-pigments were extracted in 90% acetone and quantified spectrophotometrically before and after acidification of the samples, according to Strickland and Parsons (1972). PO_4^{3-} was quantified by the colorimetric method as in Grasshoff et al. (1999). For the stable isotope composition of the DIC, the water was sampled and transferred directly to 150 mL serum vials, which were poisoned by adding 0.2 mL of a solution saturated with $HgCl_2$ and carefully sealed, taking care that no air remained in contact with samples. Vials were also stored in the dark to prevent photo oxidation. In the laboratory, the δ^{13}C-DIC signature was determined following the protocol of Bouillon et al. (2007). We injected 40 mL of helium gas inside the bottles to create a headspace, maintaining the bottles bottom-up and simultaneously expelling water by a second needle.. Then, 0.2 mL of ultrapure and concentrated H_3PO_4 was introduced to convert all inorganic carbon to CO_2. Samples were shaken vigorously and kept 12h in the dark at a controlled temperature of 25°C. The δ^{13}C of CO_2 in the headspace was determined by injecting between 0.5

mL and 1 mL of the headspace gas in an isotopic ratio mass spectrometer (IRMS, Micromass IsoPrime), equipped with a manual gas injection port. δ^{13}C-DIC was calibrated using a laboratory standard, which was prepared adding 45 mg of Na_2CO_3 in a sealed vial flushed with helium and dissolved with 3 mL of 85% H_3PO_4, as described in Deirmendjian and Abril (2018). This standard was calibrated against certified standard (NBS19, -1.96%) using a dual-inlet IRMS. The isotopic value of the Na_2CO_3 standard was -4.5±0.2‰. The obtained δ^{13}C values were corrected for the partitioning of CO_2 between the gaseous (headspace) and water phase in each sample using the algorithm of Miyajima et al. (1995). The repeatability of the analysis was approximately 0.1‰. The δ^{13}C-DIC signatures are reported in ‰ relative to the standard Vienna Pee Dee Belemnite (V-PDB) scale. TA was measured on 70 mL of filtrate samples, by the classical Gran titration method (Gran, 1952) using an automated titration system (Mettler Toledo model T50). The reproducibility of the titration was ± 3 µmol kg^{-1} (n = 5), and the accuracy was estimated at ± 5 µmol kg^{-1} (inferred from certified material reference, CRM, provided by A. G. Dickson, Scripps institution of Oceanography). To compare the pCO_2 with discrete sampling, we used the value of pCO_2 exactly the moment of the discrete sampling at the fixed station (after achievement of equilibration). As such, we obtained the values of pCO_2 and TA at same time and place. DIC concentrations were calculated from the values of pCO_2 and TA, and were very consistent with the DIC calculated from the values of measured pH and TA (Cotovicz et al. 2015). Calculations of DIC were made using the carbonic acid constants proposed by Mehrbach et al. (1973) refitted by Dickson and Millero (1987) as implemented in the CO2Calc V 4.0.9 program (Robbins et al. 2010).

2.3. Calculation of DIC and δ^{13}C-DIC addition or loss

Guanabara Bay did not present a marked saline gradient (Tab. 1; range was 14 to 35). Instead, this bay presents salinities generally higher than 30, and the low salinity waters are restricted to locations close to the river water and effluent discharges. When the river DIC inputs are weak or negligible, the conservative mixing of DIC (DIC_{mixing}) can be calculate using the marine end-member as follows (Jiang et al. 2008):

$$DIC_{mixing} = S_i/S_{ocean} * DIC_{ocean} \quad (1)$$

Where S_i is the measured salinity, S_{ocean} the salinity of the ocean end-member, and DIC_{ocean} the DIC concentration of the ocean end-member. The DIC_{mixing} is the DIC concentration after the ocean end-member is diluted by a zero DIC freshwater; however, this equation also includes possible DIC inputs from river (Jiang et al. 2008).

The excess of DIC (ΔDIC_{excess}) is defined as the DIC addition or loss relative to the conservative mixing (Jiang et al. 2008), and can be expressed as:

$$\Delta DIC_{excess} = DIC_i - DIC_{mixing} \quad (2)$$

Where DIC_i is the measured DIC. In the same way, the excess of total alkalinity (ΔTA_{excess}) can be calculated as the deviation from the conservative mixing:

$$\Delta TA_{excess} = TA_i - TA_{mixing} \quad (3)$$

In a similar approach developed by Yang et al. (2018), the difference between the δ^{13}C-DIC of the sample (δ^{13}C-DIC_i) and the δ^{13}C-DIC of the marine end-member (δ^{13}C-DIC_{ocean}) represent the

stable isotopic deviation from the marine end-member ($\Delta\delta^{13}$C-DIC) linked to local processes, as follows:

$$\Delta\delta^{13}\text{C-DIC} = \delta^{13}\text{C-DIC}_i - \delta^{13}\text{C-DIC}_{ocean} \quad (4)$$

When DIC is altered by processes of organic carbon degradation, primary production, and/or air-water exchanges, its isotopic composition is also altered, following mass balance equations (complete set of equation can be found in Yang et al. 2018). The simplified equation is:

$$\Delta\delta^{13}\text{C-DIC} = \Delta\text{DIC}_{excess}/\text{DIC}_i*(\delta^{13}\text{C}_{excess}-\delta^{13}\text{C}_{ocean}) \quad (5)$$

The $\delta^{13}C_{excess}$ represent the stable isotopic composition of the added or lost DIC whereas the $\delta^{13}C_{ocean}$ is the stable isotopic composition of the marine end-member. In coastal waters with limited river inputs, the DIC_i and DIC_{ocean} are approximately the same. Then, the equation 5 can be adjusted to:

$$\Delta\delta^{13}\text{C-DIC} = \Delta\text{DIC}_{excess}/\text{DIC}_{ocean}*(\delta^{13}\text{C}_{excess}-\delta^{13}\text{C}_{ocean}) \quad (6)$$

This equation above means that $\Delta DIC_{excess}/DIC_{ocean}$ and $\Delta\delta^{13}$C-DIC are linked and linearly related. In this way, the slope of this relationship can be used to infer the isotopic composition of the added or lost DIC and the ocean end-member value (Yang et al. 2018).

The δ^{13}C signature of the added or lost DIC due to the organic carbon production or respiration was taken as the average of δ^{13}C-POC value in the bay, which is about -20‰ (Kalas et al. 2009). The fractionation factor (αCO_2) due to outgassing of CO_2 was calculated following the procedures described by Alling et al. (2012) and Samanta et al. (2015). We applied the equation of Rau et al. (1996) to estimate the fractionation factor (α) between DIC and the dissolved CO_2 in water, according to:

$$\delta^{13}\text{C-CO}_2 = \delta^{13}\text{C-DIC} + 23.644 - 9701.5/T \quad (7)$$

This equation gives the equilibrium fractionation factor (εCO_2), which is the difference between δ^{13}C-CO_2 and δ^{13}C-DIC. This calculation provides a value of εCO_2 of -9.2‰, representing the averaged found in the sector 2 (the only sector that is a net source of CO_2 to the atmosphere). Defining fCO_2 as the fraction of DIC remaining in the water after outgassing of CO_2, we can calculate the DIC concentration after CO_2 loss (DIC_F, which is equivalent to the measured DIC, DICi), according:

$$\text{DIC}_F = fCO_2 * \text{DIC}_I \quad (8)$$

where DIC_I represents the initial DIC concentration before outgassing, which is equivalent to the calculated DIC based on equation 1, DIC_{mixing}. The $^{13}C/^{12}C$ ratio in the remaining waters (R_F) will be fractionated during progressive outgassing by the Rayleigh distillation process, according:

$$R_F = R_I\ (fCO_2)^{\alpha CO2-1} \quad (9)$$

Where R_I is the initial $^{13}C/^{12}C$ ratio before outgassing. This equation is equivalent to (Alling et al. 2012):

$$\delta^{13}C_F = \delta^{13}C_I + 10^3\ (\alpha_{CO2} - 1)\ \ln(f_{CO2}) \quad (10)$$

If we consider that the amount of DIC that is lost by outgassing is small compared to the total pool of DIC (Alling et al. 2012; Samanta et al. 2015), the DIC_F tend to be close to DIC_{mixing} (in fact this ratio is close to 1 in Guanabara Bay, and consistent with other studies). In this way, equations 1, 4, 8 and 9 can be combined:

$$\Delta\delta^{13}C\text{-}DIC \sim \Delta DIC_{exccess} (\alpha_{CO2} - 1)10^3 \quad (11)$$

Considering that $\alpha CO_2 \sim 0.991$ in Guanabara Bay, there is a near linear relationship between $\Delta\delta^{13}C$-DIC and ΔDIC_{excess}, with a slope of -9.2 value of outgassed CO_2. As the bay is a net sink of CO_2 (Cotovicz et al. 2015), we also calculate a slope representing the uptake of atmospheric CO_2. During uptake, $\alpha CO_2 \sim 0.998$ (Siegethaler and Münnich, 1981; Inoue and Sugimura, 1985), giving a slope of approximately -2.0 that represents the process of CO_2 uptake.

The average $\delta^{13}C$ -DIC signature of the wastewater DIC input was calculate with the keeling plot for the most polluted region (Fig. S1, supplementary file), which give a value of -12.2‰. This stable isotopic signature is very consistent with that found in wastewater samples (-12.0‰).

2.4. Estimates of the apparent photosynthetic fractionation factor of DIC (ε-DIC)

Photosynthesis leads to the ^{13}C enrichment of the remaining DIC pool as the phytoplankton uses preferentially the ^{12}C (Mook 2001). The photosynthetic fractionation factor of DIC consumed (ε_p-DIC) was calculated using the diurnal variations in the DIC concentrations and its stable isotope composition. In Sep.2013, Jan.2014 and Apr.2014, diurnal variations in water $\delta^{13}C$-DIC were estimated within the upper sectors (sector 4 and 5) by performing lateral trajectories back and forth across the sectors from dawn to noon (further referred as morning period) and from noon to dusk (further referred as afternoon period). The stable isotope composition of the DIC used by phytoplankton ($\delta^{13}C_{used}$) from dawn to noon period is likened to the DIC concentrations and its stable isotope composition observed between these two periods considering a simple conservative mixing by a mass balance equation:

$$\delta^{13}C_{used} = (DIC_{dawn}\delta^{13}C_{dawn} - DIC_{noon}\delta^{13}C_{noon}) / (DIC_{dawn} - DIC_{noon}) \quad (12)$$

where $\delta^{13}C_{dawn}$ and $\delta^{13}C_{noon}$ refer to the stable isotope composition of the DIC at dawn and noon, respectively, and DIC_{dawn} and DIC_{noon} refer to their respective concentrations. This formulation was also applied to investigate the stable isotope composition of the DIC used by phytoplankton during the afternoon. Then, this apparent photosynthetic fractionation of DIC (ε_p-DIC) was then estimated as the difference between the initial composition of DIC ($\delta^{13}C$-DIC_i) and the calculated $\delta^{13}C_{used}$ for each period (morning and afternoon), as follows:

$$\varepsilon_p\text{-}DIC = \delta^{13}C\text{-}DIC_i - \delta^{13}C_{used} \quad (13)$$

In addition, we calculated the plots of Rayleigh Distillation, where the increase in $\delta^{13}C$-DIC was plotted against the consumed DIC at the diel scale, in a similar approach of Dam et al. (2018).

2.5. Statistical Analysis

The Shapiro-Wilk test showed that data of pCO_2, TA, DIC, $\delta^{13}C$-DIC and Chl *a* did not follow a normal distribution. Consequently, non-parametric statistical tests were performed. The paired

Wilcoxon test was used to compare concentrations of the measured parameters between surface and bottom waters. The seasonal differences were analyzed by the Mann-Whitney test. Spearman rank coefficient was used to calculate the coefficient correlations between the measured parameters. Linear and non-linear (second order polynomial) regressions were also calculated. All statistical analysis were based on $\alpha = 0.05$ and were performed with the GraphPad Prism 6 software.

2.6. Data Compilation and Literature Survey

A compilation of δ^{13}C-DIC signatures from global databases such as the *Institute National des Sciences de L'Univers* (INSU-France) and the Carbon Dioxide Information Analysis Center (CDIAC) was carried out to obtain δ^{13}C-DIC data of other estuarine, coastal and open ocean waters worldwide. We also used the search engines Google Scholar and Web of Science to compile data from literature. We recorded the available data directly from tables and/or interpolated from figures using the data extraction program PlotDigitalizer. The different δ^{13}C-DIC data obtained from this compilation work were ranked according to their salinity in order to compare it with the data obtained in this study.

3. Results

The Table 1 showed the average concentrations with standard deviations as well as the ranges of the main water parameters analyzed in this study, separated by sectors. The upper sectors of the bay (sectors 4 and 5) presented lower salinities (27 ± 4.3 and 27.2 ± 3.5, respectively) and higher temperatures (26.8 ± 2.6 °C and 26.7 ± 2.2 °C, respectively), associated to waters with longest residence times (Tab. 1). To the contrary of upper sectors, sector 1 which is located near the mouth of the bay, showed lower temperatures (23.8 ± 1.7 °C) and higher salinities (32.2 ± 2.1) as expected due to the major influence of shelf waters.

	Sector 1	Sector 2	Sector 3	Sector 4	Sector 5
Temperature (°C)	23.8 ± 1.7 (21.0 – 29.3)	25.5 ± 2.2 (22.1 – 32.4)	25.4 ± 2.1 (22.1 – 31.5)	26.8 ± 2.6 (22.0 – 32.3)	26.7 ± 2.2 (22.6 – 33.9)
Salinity	32.2 ± 2.1 (25.4 – 34.9)	30.3 ± 2.4 (17.7 – 33.7)	29.8 ± 3.0 (15.1 – 33.8)	27.0 ± 4.3 (14.6 – 33.2)	27.2 ± 3.5 (16.6 – 32.9)
δ^{13}C-DIC (‰)	1.59 ± 0.84 (-0.02 / 3.03)	0.43 ± 1.93 (-6.17 / 3.24)	1.68 ± 1.25 (-1.88 / 4.57)	1.15 ± 1.50 (-2.50 / 3.81)	(0.99 ± 1.66) (-4.87 / 3.71)
pCO_2 (ppmv)	411 ± 145 (104 – 747)	711 ± 561 (50 – 3715)	286 ± 157 (41 – 660)	307 ± 256 (29 – 2222)	272 ± 293 (22 – 2203)
pH (NBS)	8.20 ± 0.16 (7.90 – 8.71)	8.15 ± 0.32 (7.33 – 8.96)	8.35 ± 0.23 (7.88 – 8.96)	8.34 ± 0.29 (7.39 – 9.01)	8.44 ± 0.31 (7.51 – 9.23)
TA ($\mu mol.kg^{-1}$)	2240 ± 92 (1942 - 2320)	2291 ± 99 (1890 - 2488)	2168 ± 177 (1507 - 2500)	2045 ± 369 (2111 - 3920)	2137 ± 166 (1479 - 2314)
DIC ($\mu mol.kg^{-1}$)	1985 ± 120 (1720 - 2127)	2044 ± 268 (1526 - 2523)	1847 ± 257 (1332 - 2290)	1658 ± 259 (1095 - 2118)	1758 ± 264 (1198 - 2190)
DO (%)	103 ± 29 (48 - 221)	97 ± 59 (2 - 263)	138 ± 51 (56 - 357)	142 ± 62 (30 - 361)	160 ± 69 (46 - 370)
Chl-*a* ($\mu g.L^{-1}$)	19.1 ± 22.0 (2.0 - 128.0)	46.2 ± 51.4 (3.3 - 212.9)	57.6 ± 90.0 (1.6 - 537.2)	69.2 ± 60.2 (13.1 - 288.8)	107.7 ± 101.8 (1.5 - 822.1)
PO_4^{3-}-P (µM)	1.11 ± 0.60 (0.11- 2.44)	5.28 ± 3.88 (0.17 - 20.79)	1.51 ± 1.07 (0.17 - 1.10)	1.10 ± 0.79 (0.03 - 2.96)	2.23 ± 2.17 (0.02 - 8.72)

Table 1: Mean (± standard deviation) and ranges of the principal parameters investigated in the waters of Guanabara Bay, separated by sectors.

The δ^{13}C-DIC signatures in Guanabara Bay did not present conservative distributions with salinity gradient (Fig. S2; supplementary file). Indeed, DIC in the bay was enriched in ^{13}C in some parts (mainly sectors 3, 4 and 5) relative to the marine end-member that presented a stable isotopic signature of 1.5‰ (Tab. 1), whereas in some restricted parts the bay showed ^{13}C depletion (mainly sector 2) (Tab. 1, Fig. 1). Spatially, the sectors 1 and 3 presented the higher averages of δ^{13}C-DIC signatures, which were 1.6‰ and 1.7‰, respectively (Tab. 1). However, some extreme high values (δ^{13}C-DIC > 3‰) were also present at the most shallow-confined regions of the bay (sectors 4 and 5) (Tab. 1). Sector 2, the most polluted region, presented the lowest average of δ^{13}C-DIC, which was 0.4‰ (Tab. 1). Some more negative values of δ^{13}C-DIC were also found in sectors 4 and 5 close to the outlet of rivers and urban sewage networks (Tab. 1; Fig. 1). Considering all sectors, the range of δ^{13}C-DIC signature in the entire bay was -6.1‰ (Sector 2) to 4.6‰ (Sector 3). Temporally, the δ^{13}C-DIC also showed important seasonal variations, especially between winter and summer periods (Fig. 1). Significantly (Mann-Whitney test, $p < 0.001$), the summer period (considered the months of Apr. 2013, Jul. 2013, Aug. 2013, Sep. 2013 and Ap. 2014) presented more positive δ^{13}C-DIC signatures than the winter period (Oct. 2013, Dec. 2013, Jan. 2014 and Feb. 2014). Indeed, the average signatures of δ^{13}C-DIC for the entire bay in winter and summer were respectively 1.0‰ ± 1.4‰ and 1.5‰ ± 1.7‰. Moreover, the differences between surface and bottom waters for δ^{13}C-DIC during summer were of high statistical significance ($p < 0.001$; Wilcoxon test). DIC pool was significantly enriched in ^{13}C at the surface layer, as δ^{13}C-DIC averaged at 1.8‰ ± 0.6‰ in surface waters and 1.2‰ ± 1.0‰ in bottom waters (Tab. S1, supplementary file).

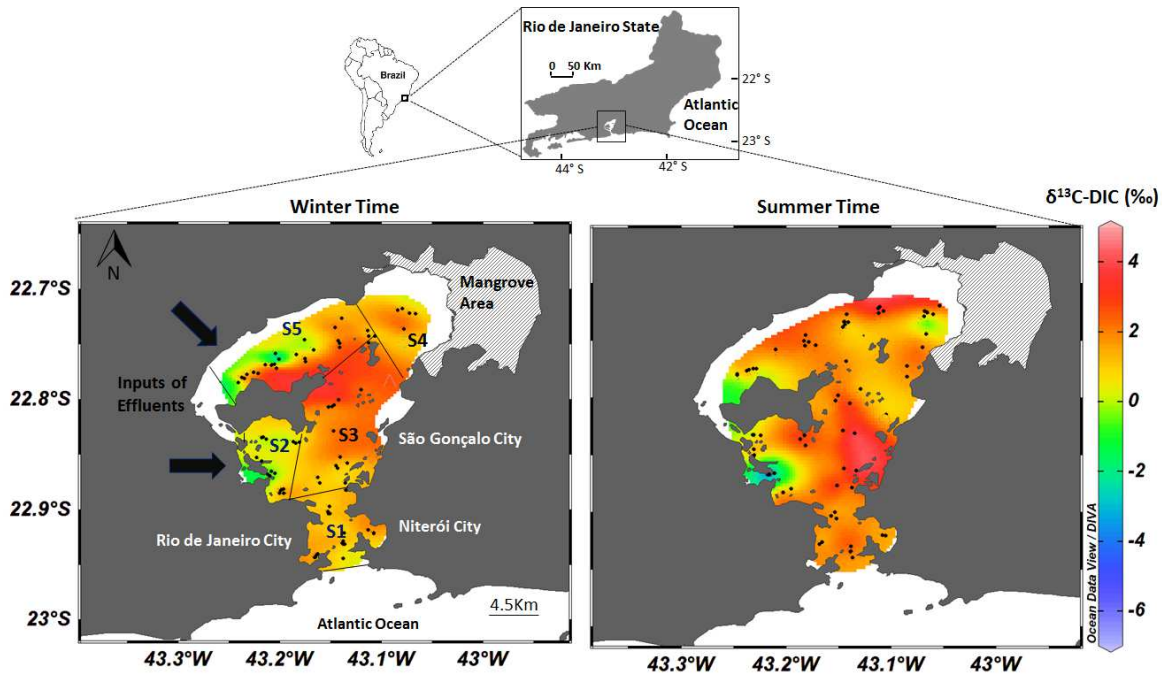

Figure 1. Composite maps showing the study area and the spatial distributions of the δ^{13}C-DIC signatures in winter period (a) and summer period (b) in surface waters of the Guanabara Bay. The bay was divided into five sectors (S1 to S5). The black dots represent the sampled sites.

The Spearman correlation matrix was calculated for all the parameters considered in this study: δ^{13}C-DIC, salinity, temperature, Chl *a*, DIC, pCO_2, DO, photosynthetically active radiation (PAR), suspended particulate material (SPM), and particulate organic carbon (POC) (Tab. S2, supplementary file). The values were established with averages for each sampling campaign. Interestingly, δ^{13}C-DIC was significantly and positively correlated to temperature, Chl *a*, PAR, DO, SPM and POC concentrations, while negatively correlated to pCO_2 levels and DIC concentrations.

Fig. 2 showed the calculated diel photosynthetic fractionation factor (ε-DIC) plotted against the discrete values of pCO_2 and DIC concentrations. This approach was applied only at the diel scale, assuming that the phytoplankton blooms realized isotopic fractionation by incorporating preferentially the lighter stable carbon isotope. We compare the fractionation between the morning and the afternoon. The isotopic fractionation was higher during the morning, ranging from 18.7‰ to 21.6‰ whereas lower fractionations occurred during the afternoon, and ranged between 6.8‰ to 11.1‰ (Fig. 2). The photosynthetic fractionation factor was strongly and positively correlated to the concentrations of DIC ($R^2 = 0.73$, $p = 0.02$) and pCO_2 ($R^2 = 0.88$, $p < 0.005$) (Fig. 2). Fig. 3 showed the plots of Rayleigh distillation that aimed to better analyze the diel isotopic fractionation dynamic. The increase of δ^{13}C-DIC was related to a given change in the fraction of consumed DIC. The diel cycles of production and respiration caused δ^{13}C-DIC to vary between 2.1‰ and 2.8‰ (Fig. 3). The increase of δ^{13}C-DIC signatures along the day was proportional to the decrease of DIC concentrations (Fig. 3). The relationship between δ^{13}C-DIC and the Chl *a* concentrations was plotted using the sector-averaged values for each sampling survey (Fig. 4). This figure shows a positive relationship between the phytoplankton biomass and δ^{13}C-DIC, especially at the most productive regions of Guanabara Bay (sectors 3, 4 and 5), where the extreme positive δ^{13}C-DIC signatures occurred in dense phytoplankton blooms with Chl *a* concentrations above 50 µg L^{-1} (Fig. 4).

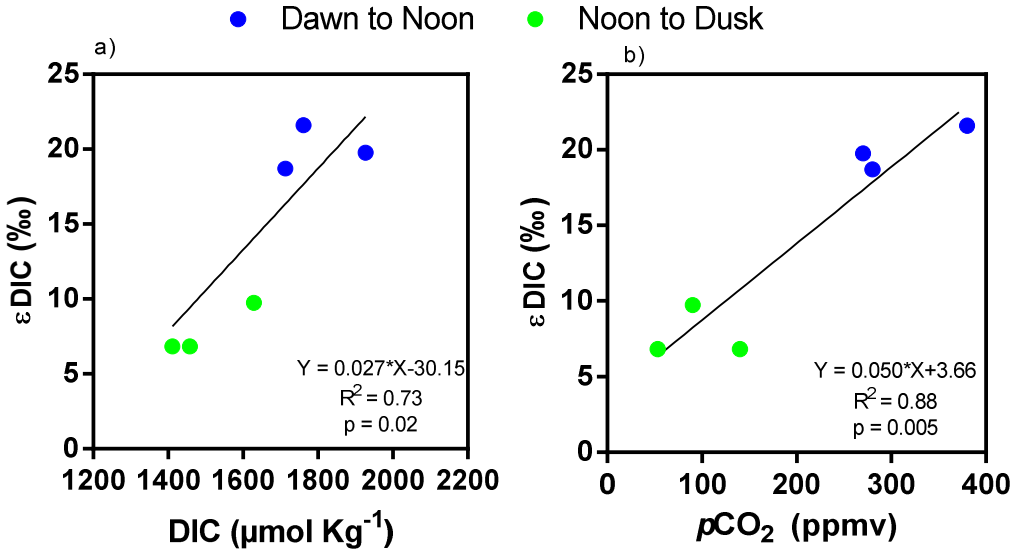

Figure 2. Calculated apparent diel phytoplankton fractionation of δ^{13}C-DIC (ε-DIC) plotted against a) pCO_2 values and b) DIC concentrations. The blue circles represent the ε-DIC for the period from dawn to noon, and the green circles represent the ε-DIC for the period from noon to dusk.

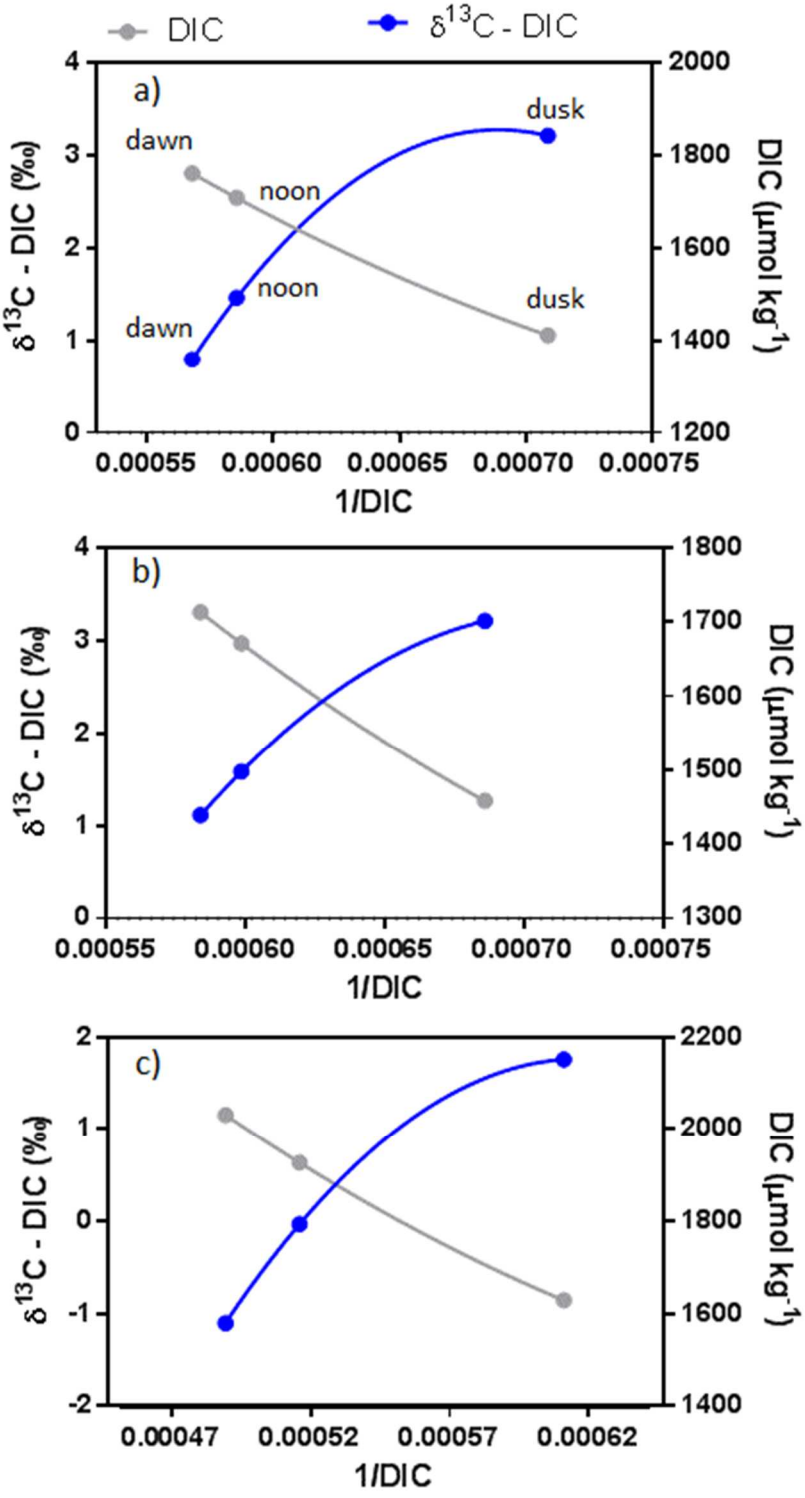

Figure 3. Plots showing the diel variations of δ13C-DIC and DIC (Rayleigh Distillation), where the increases of δ^{13}C-DIC values are equivalent to decreases in the DIC concentrations. Graphs a, b and c are represent the diel surveys (from dawn to dusk) in the months of Sep.2013, Jan.2014 and Apr.2014, respectively.

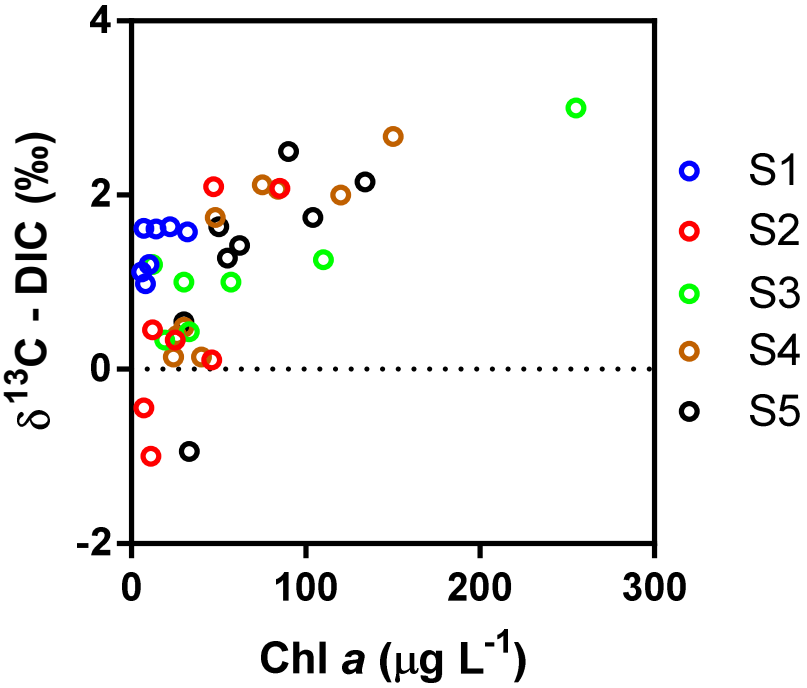

Figure 4. Relationship between δ^{13}C-DIC signatures and Chl a concentrations. The graph present the averaged-sector values for each sampling campaign.

The comparison of δ^{13}C-DIC signatures of Guanabara Bay with other ecosystems worldwide was provided in Fig. 5. Guanabara Bay showed an inverse tendency between δ^{13}C-DIC and pCO_2 values (Fig. 5a), where phytoplankton-dominated waters presented the highest δ^{13}C-DIC and the lowest pCO_2 values. The values of pCO_2 in Guanabara Bay were generally lower than the compiled data, whereas δ^{13}C-DIC signatures were much higher (Fig. 5a). This comparison of Guanabara Bay with other coastal and open ocean waters worldwide was also performed considering the salinity (Fig. 5b and 5c). These graphs showed a high scattering in the distributions of the δ^{13}C-DIC according to salinity. For a same salinity, the δ^{13}C-DIC may exhibit variation up to 20‰. The range of δ^{13}C-DIC was higher in low salinity regions and decreased progressively when freshwaters mixed with ocean waters. The salinity range between 20-30 presented the highest δ^{13}C-DIC enrichment in Guanabara Bay compared to the data from other estuaries and coasts, with a difference of about 3.20‰, on average (Fig. 5b). Compared to mangrove-dominated estuaries with salinities ranging from 15 to 20, Guanabara Bay showed an significant (Mann Whitney test, $p < 0.0001$) increase in δ^{13}C-DIC of 6.75‰ (Fig. 5b).

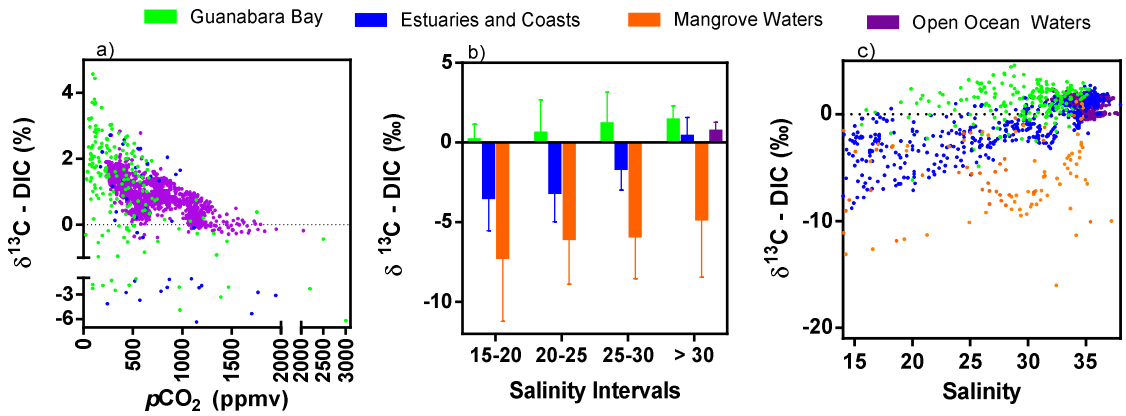

Figure 5. Comparison of Guanabara Bay with other systems worldwide: a) relationship between δ^{13}C-DIC and pCO_2 values; b) distributions of δ^{13}C-DIC according to salinity intervals; c) distributions of δ^{13}C-DIC values against salinity. The references of the compiled data set are provided in the supplementary file.

4. Discussion

4.1 Sewage inputs of depleted δ^{13}C-DIC

As a coastal embayment dominated by saline waters, the inputs of freshwater to Guanabara Bay are very low compared to its water volume (Kjerfve et al. 1997). Taking account this hydrological characteristic, we calculated the sinks and sources of DIC and TA to the system for a special case, i.e., when the freshwater inputs are weak, following the procedures described by Jiang et al. (2008). Thus, it is possible to infer the gains and losses of DIC (ΔDIC_{excess}) and TA (ΔTA_{excess}) relative to the conservative mixing (see materials and methods for details). The maximum values of ΔDIC_{excess} and ΔTA_{excess} were coincident with the highest values of pCO_2 and no related to salinity (Fig. S2; supplementary file). Oversaturation of pCO_2 in the bay was restricted to sites close to the small river mouths and sewage channels (Cotovicz et al. 2015). These polluted sites present occasional occurrence of hypoxia and anoxia events, sustaining heterotrophic metabolism (Ribeiro and Kjerfve, 2002; Cotovicz et al. 2015). Anaerobic processes including ammonification, denitrification and sulphate reduction can contributes to the production of alkalinity (Abril and Frankignoulle, 2001; Hu and Cai, 2011).

The spatial distributions of δ^{13}C-DIC along Guanabara Bay shows a higher ^{13}C depletion (down to -6.17‰) only closest to the locations that receive these direct inputs of DIC from effluent discharges (Fig. 1). Fig. 6 shows the plot of $\Delta DIC_{excess}/DIC_{ocean}$ against $\Delta\delta^{13}$C-DIC, and the slopes of this relationship can be used to infer the main biogeochemical processes affecting the distributions of DIC and δ^{13}C-DIC (see the figure caption for further explanations). The highest DIC additions occurred closest to Rio de Janeiro city at the northwestern region of Guanabara Bay (Sector 2). These samples from polluted sites fall within the III quadrant of the graph, indicating processes of organic carbon degradation (Samanta et al. 2015; Yang et al. 2018). For very high pCO_2 values, the data in quadrant III follows the theoretical slopes of wastewater contribution (slope = -0.012; vector D) and the degradation of organic carbon (slope = -0.020; vector C), and confirms the DIC inputs more depleted in ^{13}C. These polluted regions present the

highest bacterial and virus contents (Fistarol et al. 2015), are sources of CO_2 and CH_4 (Cotovicz et al. 2015; 2016b), and show episodic evidence of corrosive waters with low saturation state of calcium carbonates (Cotovicz at el., 2018b). Similar results were found in the urbanized temperate Jiaozhou Bay-China (Yang et al.; 2018), where the authors found an important input of depleted δ^{13}C-DIC in waters that receive direct discharge from wastewater plans.

The strong negative correlation ($R^2 = 0.8$; p-value<0.001) between δ^{13}C-DIC and PO_4^{3-} in sector 2 reinforce the role of wastewaters as the main source of PO_4^{3-} and DIC depleted in ^{13}C in this region (Fig. S3; supplementary file). Studies have shown that, in general, the PO_4^{3-}-P was the dominant limiting nutrient in the bay, presenting sometimes an almost depletion and related to the strong phytoplankton uptake (Costa-Santos 2015; Brandini et al. 2016). The calculated isotopic signature of the added DIC for the samples located in these polluted regions (excluding the data with Chl *a* concentrations > 50 µg L^{-1}) gives a stable isotopic signature of sewage source of -12.2‰ (Fig. S2). This value is very consistent with that found in wastewater treatment plants in China (average of -12‰; Yang et al. 2018), and with values found in a domestic sewage emissary in another region of Rio de Janeiro city (-13‰; unpublished data). Taking into account this, we quantified the contribution of sewage discharges for the two most polluted regions (sectors 2 and 5; Fig. 1) by applying a simple two-source mixing model (Phillips and Gregg, 2001). We used the value of -12.2‰ as the δ^{13}C-DIC signature of sewage source, and the value of 1.5‰ as the δ^{13}C-DIC-signature source of marine source (considered the average δ^{13}C-DIC signature of sector 1). The model calculated a sewage contribution of about 10% in sector 2 and 5% in sector 5. The depleted δ^{13}C-DIC signature from polluted sources is lost very fast in the bay, confirming the sewage-derived DIC is rapidly degassed and/or assimilated by phytoplankton blooms, as we will discuss in the next section of the manuscript. Important to point that the degassing is a process that turns the water more enriched in the heavier carbon isotope (^{13}C), since that during CO_2 emissions the lighter carbon (^{12}C) is preferentially emitted due to the kinetic isotope effect.

Another source of DIC depleted in ^{13}C to the water column in Guanabara Bay could be the mangrove forest located at the northeastern region (Fig. 1); however, we could not find a clear contribution into the bay (except for one sample collected close to the region, during low tide, which presented a negative δ^{13}C-DIC signature of -2.5‰). This value is very far from that found in mangrove-dominated waters, for example, in a tidal creek in Gazi Bay (Kenya) where the δ^{13}C-DIC values were very depleted (~ -8‰) even for salinities higher than 30 (Bouillon et al. 2007) (Fig. 5). This low influence of mangrove in Guanabara Bay occurs probably because of low tidal pumping related to the microtidal character of the bay (Cotovicz et al. 2018a). In addition, the less ^{13}C-enriched sediments were restricted to the area very close to the mangrove forest (Carreira et al. 2002).

4.2 Influence of the phytoplankton fractionation on the δ^{13}C-DIC dynamics

Despite the influence of wastewater contribution closest to sites that receive direct sewage discharge, most of δ^{13}C-DIC values are positive, indicating an isotopic fractionation of DIC by marine phytoplankton by a preferential use of ^{12}C during photosynthesis (Fig. 6). Many data points follow the theoretical slope of primary production (represented by vector A) that decreases the ratio $\Delta DIC_{excess}/DIC_{ocean}$ and increases the $\Delta\delta^{13}$C-DIC in the quadrant I (slope of -0.020). The high incidence of PAR, especially during summer, associate with high nutrient availability and

formation of thermohaline stratification, increases the rates of primary production (Rebello et al 1988), associated with development of massive phytoplankton blooms and strong CO_2 uptake (Cotovicz et al. 2015). This uptake of DIC removes preferentially the lighter ^{12}C, enriching the waters with the heavier stable carbon isotope (Mook, 2001). Successive algal blooms could consumes more of the DIC pool, and the residual DIC becomes progressively ^{13}C-enriched due to the isotopic fractionation (Finlay and Kendall, 2007). Guanabara Bay showed persistent phytoplankton blooms in all the sampling campaigns, which spread to the entire bay and cover larger areas during summer months (Cotovicz et al. 2015). Fig. 4 corroborates this result, with a positive tendency between the $\delta^{13}C$-DIC and Chl *a* concentrations, suggesting that the seasonal variation of the $\delta^{13}C$-DIC signature is related to changes in the extension of the phytoplankton dominance. This feature was also reported in the Perdido Estuary (Florida, USA) during periods of higher phytoplankton production (Coffin and Cifuentes 1999), in the Scheldt Estuary (Netherlands and Belgium) when the $\delta^{13}C$-DIC showed higher signatures during phytoplankton bloom periods (Hellings et al. 2001; Gillikin et al. 2006).

Fig. 6 present some points located in the quadrant IV, which represents the carbonate dissolution. The process of carbonate dissolution consumes DIC of the water column, and adds $\delta^{13}C$ with an isotopic signature closest to that of marine carbonates (0‰), turning the waters enriched in ^{13}C relative to the conservative mixing (Alling et al. 2012). However, this process is unlikely to occur in the bay since that the values of pCO_2 in quadrant IV are low and the pH values are high (Cotovicz et al. 2018b). Actually, DIC and $\delta^{13}C$-DIC can be subjected simultaneously to more than one process and not just by a specific one (Samanta et al. 2015). This means that if one sample was subject to degradation of organic carbon (represented by quadrant III) followed by primary production (represented by quadrant I), this sample could finally be located in quadrant IV (the deviation is represented by the blue arrow, which is drawn parallel to vector A). Similarly, if a sample was subject to the DIC uptake by primary production (vector A) and thereafter occurs an intrusion of atmospheric CO_2 due to the gradient at the air-water interface (CO_2 sink, vector E), this sample could also be deviated to the quadrant IV (green arrow). The red arrow is drawn parallel to vector B, representing the effect of organic carbon degradation followed by outgassing of CO_2. This is probably occurring in samples mainly from sector 2 that are located on quadrant IV that present high values of measured pCO_2, when the outgassing could be important due to important air-water gradient of CO_2. Another example is the quadrant I, where exists two vectors (A and B), representing the slopes of biological production and outgassing, respectively. Both these processes lead to loss of DIC and increase of $\delta^{13}C$-DIC. However, the process of outgassing in these samples are unlikely since that the values of pCO_2 in this quadrant are highly under-saturated.

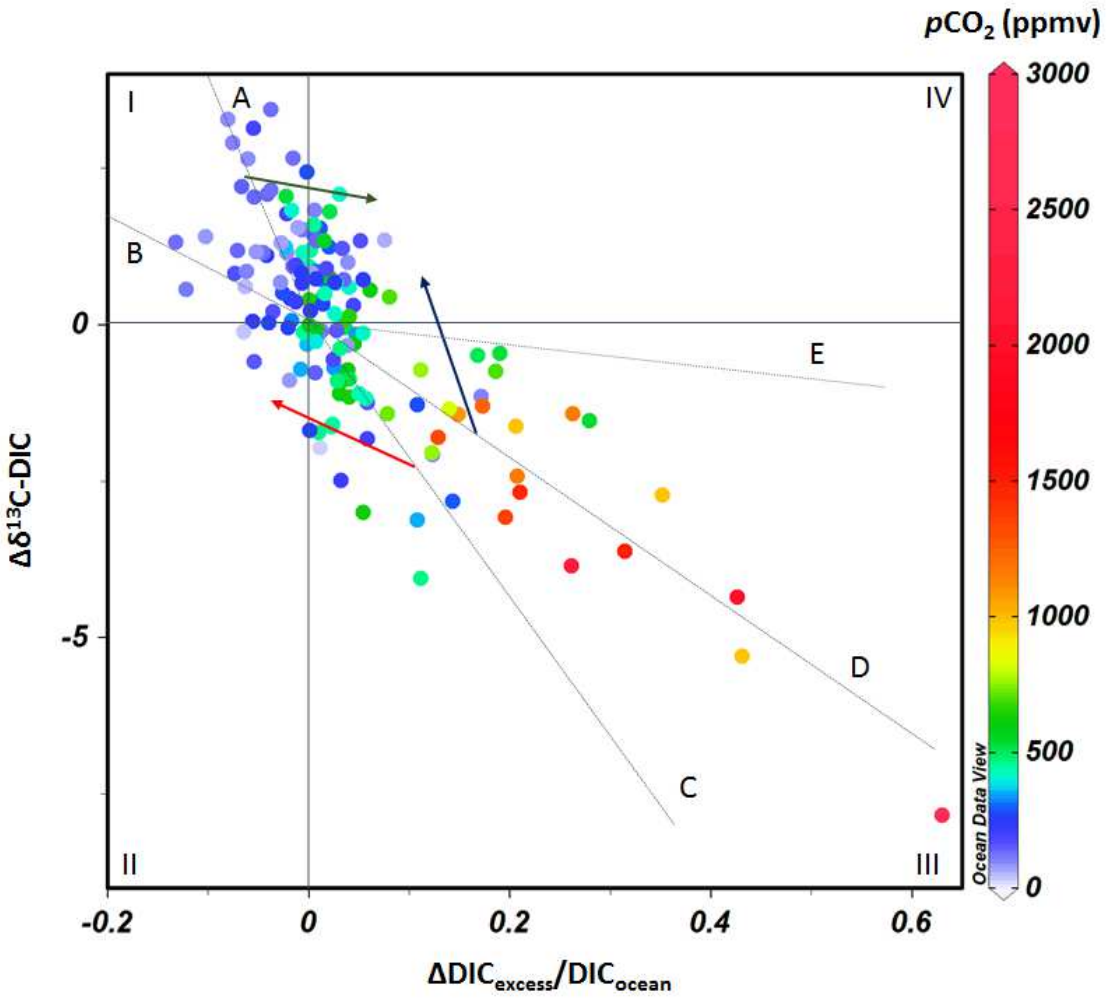

Figure 6. Plot of $\Delta\delta^{13}$C-DIC vs. $\Delta DIC_{excess}/DIC_{ocean}$ in the Guanabara Bay. The origin represents the conservative mixing with sample values equal to the ocean end-member value (see material and methods for further explanation). The four quadrants (I, II, III and IV) indicate additional processes than could influence the DIC and δ^{13}C-DIC distributions. The quadrant I represents the primary production / outgassing of CO_2, when DIC concentrations increase and δ^{13}C-DIC values decrease. The quadrant II represents the calcite precipitation, when DIC concentrations and δ^{13}C-DIC values decrease. The quadrant III represents the degradation of organic carbon and inputs from wastewater, when DIC concentrations increase and δ^{13}C-DIC decrease. The quadrant IV represents the carbonate dissolution, when the DIC concentrations and the vales of δ^{13}C-DIC increase. The vectors A, B, C, D and E represent the slopes of specific processes affecting the DIC and δ^{13}C-DIC distributions, that are, respectively, primary production (slope = -20.0‰), the outgassing of CO_2 (slope = -9.2‰), degradation of organic carbon (slope = -20.0‰), wastewater input of DIC (-12.2‰) and intrusion of atmospheric CO_2 (slope = -2.0‰). The red, blue and green arrows represent the direction in which the samples will follow if they are subject to more than one process. The red arrow represents the effect of organic matter degradation followed by outgassing of CO_2, which is drawn parallel to vector B. The blue arrow represents the effect of degradation of organic carbon followed by biological production, which is drawn parallel to vector A. The green arrow represents the effect of primary production followed by intrusion of atmospheric CO_2 due to the air-water gradient, which is drawn parallel to vector E.

The apparent phytoplankton isotopic fractionation (ε-DIC) was higher under conditions of high availability of dissolved CO_2, with higher fractionation during the morning than the afternoon (Fig. 2). During morning, the values of pCO_2 were higher in Guanabara Bay as the results of the accumulated CO_2 respired during the nighttime (Cotovicz et al. 2015). This suggests that the discrimination against ^{13}C is higher when the availability of dissolved CO_2 is higher. Previous studies showed similar results, both in culture experiments (Fogel and Cifuentes, 1993), and *in situ* at a Chinese hypereutrophic lake (Van Dam et al. 2018). The $\delta^{13}C$-DIC fractionation by phytoplankton in Guanabara Bay follows a Rayleigh distillation (Fig. 3), where the increasing removal of DIC fractions is accompanied by the isotopic fractionation of $\delta^{13}C$-DIC, turning the water enriched in ^{13}C. The values of ε-DIC found during the morning period in Guanabara Bay were about 20‰, a classical value for the marine phytoplankton (Fontugne and Duplessy, 1981, Fogel and Cifuentes, 1999; Mook, 2001). Under conditions of low pCO_2, the $\delta^{13}C$-DIC fractionation decreases during the afternoon, reflecting the decline in carbon assimilation efficiency. This decrease of fractionation under CO_2 limitation was showed experimentally for marine diatoms (Burkhardt et al. 1999), and it is consistent with results found in a hypertrophic Chinese lake under conditions of CO_2 sub saturation (Van Dam et al. 2018). In addition, under low availability of dissolved CO_2, the phytoplankton can consumes bicarbonate (HCO_3^-) (Burns and Beardall, 1987), and this could contribute to decrease the isotopic fractionation factor since that the isotope ratio of HCO_3^- is about 8‰ more positive than that of dissolved CO_2 (Fogel and Cifuentes, 1999). Previous studies suggested an active uptake of HCO_3^- in Guanabara Bay due to the enrichment of the $\delta^{13}C$-POC pool ($\delta^{13}C$-POC reaching -15.1‰; Kalas et al. 2009; Martins et al. 2016). Cyanobacteria blooms, which have already been documented in Guanabara Bay, can use bicarbonate under low pCO_2 availability (Miller et al. 1990).

4.3 Comparison with other ecosystems worldwide

The plot of $\delta^{13}C$-DIC versus pCO_2 (Fig. 5a) shows that the blooms-dominated waters present strong pCO_2 under-saturation and are as well enriched in ^{13}C, that is intrinsically related to the extreme levels of primary production. Guanabara Bay presented values of $\delta^{13}C$-DIC high above than those of the compiled data in estuaries and coasts, revealing the advanced process of eutrophication in the bay. The compiled data in estuaries presented a high scattering compared to the open ocean waters, especially for values of $\delta^{13}C$-DIC lower than 0‰ (Fig. 5c). This reflects a combination of processes such as respiration of terrestrial organic carbon from multiple sources with different $\delta^{13}C$ signatures, weathering and the contribution of carbonate rocks in the watershed, primary production, gas exchange and water mixing along the land-ocean aquatic continuum (Mook, 2001). The matrix correlation (Tab. S2) shows that higher values of $\delta^{13}C$-DIC are related to high levels of DO, POC, SPM, and Chl *a*, and low concentrations of DIC. Recent findings in Guanabara Bay showed that the DOC and POC fractions present a large phytoplankton dominance, surpassing the contribution of terrestrial sources (Cotovicz et al. 2018a). Compared to other estuaries, Guanabara Bay presented the highest enrichment of ^{13}C–DIC in the salinity range between 20 and 30 (Fig. 5b). In Guanabara Bay, this salinity interval is present in confined stratified waters of the sectors 3, 4 and 5, which are net autotrophic and phytoplankton-dominated (Rebelllo et al. 1988; Cotovicz et al. 2015; 2018a). This behavior is in contrast with most of other estuarine studies, which are mostly located in temperate regions and river-dominated ecosystems, where the effects of respiration, either in the water column or in sediments, are often much more pronounced than photosynthesis (Mook, 2001; Bouillon et al. 2003). The relative enrichment of ^{13}C–DIC is also important for salinities > 30, suggesting that Guanabara Bay can export ^{13}C-DIC

enriched waters to the coastal ocean. There is a marked depletion of δ^{13}C-DIC in estuaries dominated by mangroves. The net inputs of ^{13}C-depleted DIC in mangroves are attributed to the predominance of respiration in tidal creeks, as this process adds DIC to the water with a signature similar to that of the organic matter being respired (C3 plants with signature ranging between –24‰ to –30‰) (Bouillon et al. 2003; Bouillon et al. 2011; Miyajima et al. 2009).

In open ocean waters, the compiled data of δ^{13}C-DIC showed a range between -1.13‰ and 2.31‰, averaging at 0.70‰ ± 0.57‰ (Fig. 5). This range of δ^{13}C-DIC is in accordance with previous studies in seawaters with a limited influence from land carbon sources (-2‰ and 2‰; Mook and Tan, 1991). However, the average of 0.71‰ is slightly lower than previous averages reported in literature (Kroopnick, 1985; Mook, 2001). According to Mook (2001), the δ^{13}C-DIC in seawater varies between +0‰ and +2.5‰, with the majority of data between 1‰ and 2‰. According to Kroopnick (1985), the δ^{13}C-DIC of surface oceanic waters are generally around 2‰. Differences in the averages and ranges of these studies can be attributed to the specific conditions during sampling collection, since that consider regions with distinct biological, air-sea exchange processes and different *in situ* temperatures, which could alter the δ^{13}C-DIC signature. In addition, δ^{13}C-DIC could substantially differ considering the differences between surface and bottom waters. δ^{13}C-DIC can present vertical stratification attributed to the oxidation of the organic material produced at the surface waters (majority from phytoplanktonic origin) as it falls through the water column and remineralizes at depth, with addition of isotopically light respiratory CO_2 to the DIC pool below the pycnocline (Kroopnick, 1985, Koné et al. 2009; Eide et al. 2017). Lower δ^{13}C-DIC values in bottom waters were reported in several estuarine, coastal and open ocean waters (Chou et al 2007; Burt et al 2016; Humphreys et al. 2016; Filipsson et al. 2017). Guanabara Bay also present a significant vertical δ^{13}C-DIC stratification during summer, with higher values at surface waters, reflecting the enrichment by phytoplankton blooms, and the depletion in bottom waters due to the predominance of respiration of organic matter (Tab. S1).

5. Conclusion

Our results showed a strong control of δ^{13}C-DIC dynamics by biological processes in the highly polluted and eutrophic Guanabara Bay. Indeed, the extreme high Chl *a* concentrations concomitant with heavier δ^{13}C-DIC signatures and low pCO_2 values indicate a strong carbon isotopic fractionation by primary production, especially at mid-inner shallow regions of the bay. The isotopic fractionation induced by primary production is accentuated during summer conditions when the vertical thermohaline stratification, the nutrients availability and the photosynthetically active radiation were at their highest. Our calculated apparent phytoplankton fractionation based on diel variations of δ^{13}C-DIC signatures and DIC concentrations showed higher ^{13}C discrimination from morning to noon period, decreasing during afternoon, following a Rayleigh distillation process. Overall, the *in situ* δ^{13}C-DIC concentrations were well above than the values expected in equilibrium with atmospheric CO_2 concentrations. The lower/negative δ^{13}C-DIC signatures were restricted to the regions under direct influence of domestic effluent discharges, where high inputs of organic matter stimulate the microbial respiration that adds depleted δ^{13}C-DIC into the waters. The process of air-water exchange seems also to exert influence on the isotope signatures; however, in a lower magnitude compared to the biological activities. Compared to the compiled data from several estuaries and open ocean waters worldwide, Guanabara Bay showed a marked enrichment of ^{13}C, increasing δ^{13}C-DIC signatures. The highest signature of δ^{13}C-DIC in Guanabara Bay reached 4.57‰, and to the best of our

knowledge, this is the highest value reported in coastal and open waters worldwide. These results indicate that the eutrophication process can deeply modify the isotopic signature of the dissolved inorganic carbon pool in coastal waters dominated by large algal blooms.

Acknowledgments

This study was supported by the No Frontier Sciences Program of the Brazilian National Council of Research and Development (CNPq-PVE No 401.726/2012-6), by the Carlos Chagas Foundation for Research Support of the State of Rio de Janeiro (FAPERJ; proc. no. E-26202.785/2016), and by the Coordination for the Improvement of Higher Education Personnel (CAPES). Luiz C. Cotovicz Jr. is a postdoctoral researcher of FAPERJ (FAPERJ; proc. no. E-26202.785/2016); B. A. Knoppers is a senior scientist of CNPq (proc. no. 301572/2010-0). We are grateful to Nilva Brandini and Suzan J. Costa Santos for their support during field sampling, and to Karine Charlier for her support with IRMS analytical procedures.

References:

1 Abril, G., Frankignoulle, M., 2001. Nitrogen – alkalinity interactions in the highly polluted Scheldt Basin (Belgium). Water Res. 35, 844–850.

2 Abril, G., Richard, S., Guérin, F., 2006. In-situ measurements of dissolved gases (CH_4 and CO_2) in a wide range of concentrations in a tropical reservoir using an equilibrator. Sci. Total Environ. 354, 246–251. https://doi.org/10.1016/j.scitotenv.2004.12.051.

3 Alling, V., Porcelli, D., Mörth, C. M., Anderson, L. G., Sanchez-Garcia,L., Gustafsson, Ö. Andersson, P. S., Humborg, C., 2012. Degradation of terrestrial organic carbon, primary production and out-gassing of CO2 in the Laptev and East Siberian Seas as inferred from δ13C values of DIC, Geochim. Cosmochim. Acta. 95, 143–159, https://doi.org/10.1016/j.gca.2012.07.028.

4 Bauer, J. E., Cai, W.-J., Raymond, P., Bianchi, T. S., Hopkinson, C. S., Regnier, P., 2013. The changing carbon cycle of the coastal ocean. Nature, 504(7478), 61–70. https://doi.org/10.1038/nature12857.

5 Bhavya, P. S., Kumar, S., Gupta, G. V. M., Sudharma, K. V., Sudheesh, V., 2018. Spatio-temporal variation in δ^{13}CDIC of a tropical eutrophic estuary (Cochin estuary, India) and adjacent Arabian Sea, Cont. Shelf Res., 153, 75-85, https://doi.org/10.1016/j.csr.2017.12.006

6 Bidone, E. D., Lacerda, L. D., 2004. The use of DPSIR framework to evaluate sustainability in coastal areas, case study: Guanabara Bay Basin, Rio de Janeiro, Brazil. Reg. Environ. Change, 4, 5–16. https://doi.org/10.1007/s10113-003-0059-2

7 Borges A. V., 2005. Do we have enough pieces of the jigsaw to integrate CO_2 fluxes in the coastal ocean? Estuaries. 28, 3–27. https://doi.org/10.1007/BF02732750.

8 Borges, A. V., Abril, G., 2011. Carbon Dioxide and Methane Dynamics in Estuaries, in: Wolanski E., McLusky, D. (Eds.), Treatise on Estuarine and Coastal Science. Academic Press, Amsterdam, pp. 119–161.

9 Bouillon, S., Frankignoulle, M., Dehairs, F., Velimirov, B., Eiler, A., Abril, G., Etcheber, H., Borges, A. V., 2003. Inorganic and organic carbon biogeochemistry in the Gautami Godavari estuary (Andhra Pradesh, India) during pre-monsoon: The local impact of extensive mangrove forests. Global Biogeochem. Cycles. 17. https://doi.org/10.1029/2002GB002026.

10 Bouillon, S., Dehairs, F., Schiettecatte, L.-S., Borges, A. V., 2007. Biogeochemistry of the Tana estuary and delta (northern Kenya). Limnol. Oceanogr. 52(1), 46–59. https://doi.org/10.4319/lo.2007.52.1.0046.

11 Bouillon, S., Connolly, R. M., Gillikin, D. P., 2012. Use of Stable Isotopes to Understand Food Webs and Ecosystem Functioning in Estuaries, in: Wolanski E., McLusky, D. (Eds.), Treatise on Estuarine and Coastal Science. Academic Press, Amsterdam, pp. 143–173.

12 Brandini, N., Rodrigues, A.P.C., Abreu, I.M., Cotovicz Jr., L.C., Knoppers, B.A., Machado, W. V. 2016. Nutrient behavior in a highly-eutrophicated tropical estuarine system. Acta Limnol. Bras., 28, e-21, http://dx.doi.org/10.1590/S2179-975X3416.

13 Burkhardt, S., Riebesell, U., Zondervan, I., 1999. Effects of growth rate, CO_2 concentration, and cell size on the stable carbon isotope fractionation in marine phytoplankton. Geochim. Cosmochim. Acta. 63(22), 3729–3741. https://doi.org/10.1016/S0016-7037(99)00217-3.

14 Burns, B.D., Beardall, J., 1987. Utilization of inorganic carbon acquisition by marine microalgae. J. Exp. Mar. Biol. Ecol. 107, 75–86.

15 Burt, W. J., Thomas, H., Hagens, M., Pätsch J., Clargo, N. M., Salt, L. A., Winde, V., Böttcher, M. E., 2016. Carbon sources in the North Sea evaluated by means of radium and stable carbon isotope tracers. Limnol. Oceanogr. 61, 666–683. https://doi.org/10.1002/lno.10243.

16 Campeau A., Wallin, M. B., Giesler, R., Löfgren, S., Mörth, C. M., Schiff, S., Venkiteswaran, J. J., Bishop, K., 2017. Multiple sources and sinks of dissolved inorganic carbon across Swedish streams, refocusing the lens of stable C isotopes. Sci. Rep. 7, 1–14. https://doi.org/10.1038/s41598-017-09049-9.

17 Carreira, R. S., Wagener, A. L. R., Readman, J. W., Fileman, T. W., Macko, S. A., Veiga, A., 2002. Changes in the sedimentary organic carbon pool of a fertilized tropical estuary, Guanabara Bay, Brazil: An elemental, isotopic and molecular marker approach. Mar. Chem. 79: 207– 227. https://doi.org/10.1016/S0304-4203(02)00065-8

18 Chanton, J. P., Lewis, F. G., 1999. Plankton and Dissolved Inorganic Carbon Isotopic Composition in a River-Dominated Estuary: Apalachicola Bay, Florida. Estuaries, 22(3), 575. https://doi.org/10.2307/1353045.

19 Chen, C.-T. A., Huang, T.-H., Chen, Y.-C., Bai, Y., He, X., Kang, Y., 2013. Air–sea exchanges of CO_2 in the world's coastal seas. Biogeosciences. 10, 6509–6544. https://doi.org/10.5194/bg-10-6509-2013.

20 Chou W. C., Sheu, D. D., Lee, B. S., Tseng, C. M., Chen, C. T. A., Wang, S. L., Wong, G. T. F., 2007. Depth distributions of alkalinity, TCO2 and $\delta 13C_{TCO2}$ at SEATS time-series site in the northern South China Sea. Deep. Res. Part II Top. Stud. Oceanogr. 54, 1469–1485. https://doi.org/10.1016/j.dsr2.2007.05.002.

21 Coffin, R. B., Cifuentes, L. A., 1999. Stable Isotope Analysis of Carbon Cycling in the Perdido Estuary, Florida. Estuaries, 22(4), 917–926.

22 Costa-Santos, S. J., 2015. Determinação do estado trófico a partir da aplicação dos índices O'Boyle e TRIX nos compartimentos da Baia de Guanabara, RJ. Master Dissertation, Federal Fluminense University, Brazil. WWW Page, https://app.uff.br/riuff/bitstream/1/1642/1/Dissertacao_Suzan%20Versao_10.1_VersaoFINAL.pdf

23 Cotovicz Jr., L. C., Knoppers, B. A., Brandini, N., Costa Santos, S. J., Abril, G., 2015. A strong CO_2 sink enhanced by eutrophication in a tropical coastal embayment (Guanabara Bay, Rio de Janeiro, Brazil). Biogeosciences, 12(20), 6125–6146. https://doi.org/10.5194/bg-12-6125-2015.

24 Cotovicz Jr., L. C., Libardoni, B., Brandini, N., Knoppers, B., Abril, G. 2016a. Comparações entre medições em tempo real da pCO_2 aquática com estimativas indiretas em dois estuárioss tropicais contrastantes: o estuário eutrofizado da Baia de Guanabara (RJ) e o estuário oligotrofico

748 do Rio São Francisco (AL). Química Nova, 39, 1206-1214. https://doi.org/10.21577/0100-
749 4042.20160145.22

750 25 Cotovicz Jr., L. C., Knoppers, B. A., Brandini, N., Poirier, D., Costa Santos, S. J., Abril, G.,
751 2016b. Spatio-temporal variability of methane (CH_4) concentrations and diffusive fluxes from a
752 tropical coastal embayment surrounded by a large urban area (Guanabara Bay, Rio de Janeiro,
753 Brazil). Limnol. Oceanogr., 61, S238–S252. https://doi.org/10.1002/lno.10298.

754 26 Cotovicz Jr., L. C., Knoppers, B. A., Brandini, N., Poirier, D., Costa Santos, S. J., Cordeiro,
755 R. C., Abril, G., 2018a. Predominance of phytoplankton-derived dissolved and particulate
756 organic carbon in a highly eutrophic tropical coastal embayment (Guanabara Bay, Rio de Janeiro,
757 Brazil). Biogeochemistry, 137, 1–14. https://doi.org/10.1007/s10533-017-0405-y.

758 27 Cotovicz Jr., L. C., Knoppers, B. A., Brandini, N., Poirier D., Costa Santos, S. J., Abril, G.,
759 2018b. Aragonite saturation state in a tropical coastal embayment dominated by phytoplankton
760 blooms (Guanabara Bay - Brazil). Mar. Pollut. Bull., 0–1.
761 https://doi.org/10.1016/j.marpolbul.2017.10.064.

762 28 Deirmendjian, L., Abril, G., 2018. Carbon dioxide degassing at the groundwater-stream-
763 atmosphere interface: isotopic equilibration and hydrological mass balance in a sandy watershed.
764 J. Hydrol. 558, 129-143. https://doi.org/10.1016/j.jhydrol.2018.01.003.

765 29 Dickson, A. G., Millero, F. J., 1987. A comparison of the equilibrium constants for the
766 dissociation of carbonic acid in seawater media. Deep-Sea Res. 34, 1733–1743.

767 30 Eide, M., Olsen, A. Ninnemann, U., Johannessen, T., 2017. A Global Ocean Climatology of
768 Preindustrial and Modern Ocean $\delta^{13}C$, Global Biogeochem. Cycles,
769 https://doi.org/10.1002/2016GB005473.

770 31 Finlay, J. C., Kendall, C., 2007. Stable isotope tracing of temporal and spatial variability in
771 organic matter sources to freshwater ecosystems, in: Michener, R., Lajtha, K. (Eds.), Stable
772 isotopes in ecology and environmental science. Blackwell Publishing, Hong Kong, pp. 594.

773 32 Filipsson, H. L., McCorkle, D. C., Mackensen, A., Bernhard, J. M., Andersson, L. S.,
774 Naustvoll, L.-J., Caballero-Alfonso, A. M., Nordberg, K., Danielssen, D. S., 2017. Seasonal
775 variability of stable carbon isotopes ($\delta^{13}CDIC$) in the Skagerrak and the Baltic Sea: Distinguishing
776 between mixing and biological productivity, Palaeogeogr. Palaeoclimatol. Palaeoecol. 483, 15-
777 30. https://doi.org/10.1016/j.palaeo.2016.11.031.

778 33 Fistarol, G. O., Coutinho, F. H., Moreira, A. P. B., Venas, T., Cánovas, A., de Paula, S. E. M.,
779 Coutinho, R., de Moura, R. L., Valentin, J. L., Tenenbaum, D. R., Paranhos, R., do Valle, R. D.,
780 Vicente, A. C. P., Amado Filho, G. M., Pereira, R. C., Kruger, R., Rezende, C. E., Thompson, C.
781 C., Salomon, P. S., Thompson F. L., 2015. Environmental and Sanitary Conditions of Guanabara
782 Bay, Rio de Janeiro. Front. Front. Microbiol., 6, 1232, https://doi.org/10.3389/fmicb.2015.01232.

783 34 Fontugne, M. R., Duplessy, J.-C., 1981. Organic carbon isotopic fractionation by marine
784 plankton in the temperature range -1 to 31°C. Oecologia Acta 4(1), 85 – 90.

785 35 Frankignoulle, M., Borges, A., Biondo, R., 2001. A new design of equilibrator to monitor
786 carbon dioxide in highly dynamic and turbid environments. Water Res. 35, 1344–1347.

787 36 Fry, B., 2002. Conservative mixing of stable isotopes across estuarine salinity gradients: A
788 conceptual framework for monitoring watershed influences on downstream fisheries production.
789 Estuaries, 25(2), 264–271. https://doi.org/10.1007/BF02691313.

790 37 Gattuso J. P., Frankignoulle, M., Wollast, R., 1998. Carbon and carbonate metabolism in
791 coastal aquatic ecosystems. Annu. Rev. Ecol. Syst. 29, 405–434.
792 https://doi.org/10.1146/annurev.ecolsys.29.1.405.

793 38 Gazeau, F., Smith, S. V., Gentili, B., Frankignoulle, M., Gattuso J.-P., 2004. The European
794 coastal zone: characterization and first assessment of ecosystem metabolism. Estuar. Coast. Shelf
795 Sci. 60(4), 673–694. https://doi.org/10.1016/j.ecss.2004.03.007.

796 39 Gillikin, D. P., Lorrain, A., Bouillon, S., Willenz, P., Dehairs, F., 2006. Stable carbon isotopic
797 composition of Mytilus edulis shells: relation to metabolism, salinity, δ^{13}CDIC and
798 phytoplankton. Org. Geochem. 37(10), 1371–1382.
799 https://doi.org/10.1016/j.orggeochem.2006.03.008.

800 40 Gran, G. 1952. Determination of the equivalence point in potentiometric titrations. Part II. The
801 Analyst, 77(920), 661-671.

802 41 Grasshoff, K., Ehrhardt, M., Kremling, K., 1999. Methods of seawater analysis. Wiley-VCH.

803 42 Gruber, N., Keeling, C. D., Bacastow, R. B., Guenther, P. R., Lueker, T. J., Wahlen, M.,
804 Meijer, H. A. J., Mook, W. G., Stocker, T. F., 1999. Spatiotemporal patterns of carbon-13 in the
805 global surface oceans and the oceanic Suess Effect. Global Biogeochem. Cycles, 13(2), 307-335.

806 43 Hellings, L., Dehairs, F., Van Damme, S., Baeyens, W. 2001. 2001. Dissolved inorganic
807 carbon in a highly polluted estuary (the Scheldt), Limnol. Oceanogr., 46(6), 1406–1414.
808 https://doi.org/10.4319/lo.2001.46.6.1406.

809 44 Hu, X., Cai, W.-J., 2011. An assessment of ocean margin anaerobic processes on oceanic
810 alkalinity budget. Glob. Biogeochem. Cycles 25, n/a. http://dx.doi.org/10.1029/2010GB003859.

811 45 Humphreys, M., Greatrix, F., Tynan, E., Achterberg, E., Griffiths, A., Fry, C., Garley, R.,
812 McDonald, A., Boyce, A., 2016. Stable carbon isotopes of dissolved inorganic carbon for a zonal
813 transect across the subpolar North Atlantic Ocean in summer 2014. Earth Syst. Sci. Data, 8, 221–
814 233. https://doi.org/ 10.5194/essd-8-221-2016.

815 46 Inoue, H. and Y. Sugimura. Carbon isotopic fractionation during the CO 2 exchange process
816 between air and sea water under equilibrium and kinetic conditions. Geochim. Cosmochim. Acta,
817 49:2453-2460, 1985.

818 47 Jiang, L. Q., Cai, W.-J., Wang, Y. C., 2008. A comparative study of carbon dioxide degassing
819 in river- and marine-dominated estuaries. Limnol. Oceanogr., 53, 2603–2615.
820 https://doi.org/10.4319/lo.2008.53.6.2603.

821 48 Kalas, F. A., Carreira, R. S., Macko, S. A., Wagener, A. L. R., 2009. Molecular and isotopic
822 characterization of the particulate organic matter from an eutrophic coastal bay in SE Brazil, Cont.
823 Shelf Res., 29, 2293–2302. https://doi.org/10.1016/j.csr.2009.09.007.

824 49 Kendall, C., Doctor, D.H., 2004. Stable isotope applications in hydrologic studies, in: Drever,
825 J.I. (Eds.), Surface and ground water, weathering, and soils: Treatise on Geochemistry, v. 5, pp.
826 319-364

827 50 Kjerfve, B., Ribeiro, C. A., Dias, G. T. M., Filippo, A., Quaresma, V. S., 1997. Oceanographic
828 characteristics of an impacted coastal bay: Baia de Guanabara, Rio de Janeiro, Brazil. Cont. Shelf
829 Res. 17, 1609–1643.

830 51 Koné Y. J. M., Abril G., Kouadio K. N., Delille B., Borges A. V., 2009. Seasonal variability
831 of carbon dioxide in the rivers and lagoons of Ivory Coast (West Africa). Estuar. Coast. 32, 246–
832 260. https://doi.org/10.1007/s12237-008-9121-0.

833 52 Kroopnick, P. M., 1985. The distribution of 13C of Σ CO_2 in the world oceans, Deep Sea Res.
834 Part A, Oceanogr. Res. Pap., 32(1), 57–84. https://doi.org/10.1016/0198-0149(85)90017-2.

835 53 Kubo, A., Maeda, Y., Kanda, J. 2017. A significant net sink for CO_2 in Tokyo Bay. Sci. Rep.,
836 7, 44355. https://doi.org/10.1038/srep44355.

837 54 Mehrbach, C., Cuberson, C. H., Hawley, J. E., and Pytkowicz, R. M. 1973. Measurements of
838 the apparent dissociation constants of carbonic acid in seawater at atmospheric pressure. Limnol.
839 Oceanog., 18, 897–907, 1973.

840 55 Martins, J., Silva, T., Fernandes, A., Massone, C., Carreira, R., 2016. Characterization of
841 particulate organic matter in a Guanabara Bay- coastal ocean transect using elemental , isotopic
842 and molecular markers. PANAMJAS, 11, 276–291.

843 56 Miller, J. D., Espie, G. S. Canvin, D. T., 1990. Physiological aspects of CO_2 and HCO_3
844 transport by cyanobacteria: A review. Can. J. Bot. 68: 1291–1302. https://doi.org/10.1139/b90-
845 165.

846 57 Miyajima, T., Miyajima, Y., Hanba, Y.T., Yoshii, K., Koitabashi, T., Wada, E., 1995.
847 Determining the stable isotope ratio of total dissolved inorganic carbon in lake water by
848 GC/C/IIRMS. Limnol. Oceanog. 40, 994–1000. https://doi.org/10.4319/lo.1995.40.5.0994.

849 58 Miyajima, T., Tsuboi, Y., Tanaka, Y., Koike, I.,2009. Export of inorganic carbon from two
850 Southeast Asian mangrove forests to adjacent estuaries as estimated by the stable isotope
851 composition of dissolved inorganic carbon. J. Geophys. Res. Biogeosciences, 114(1), 1–12.
852 https://doi.org/10.1029/2008JG000861.

853 59 Mook, W.G., Tan, F.C., 1991. Stable carbon isotopes in rivers and estuaries, in: Degens, E.T.,
854 Kempe, S., Richey, J.E. (Eds.), Biogeochemistry of Major World Rivers. John Wiley and Sons,
855 Chichester, UK, pp. 245-264.

856 60 Mook, W. G., 2001. Environmental Isotopes in the Hydrological Cycle. Principles and
857 Applications. UNESCO/ IAEA Series, Paris.

858 61 Phillips, D.L., Gregg, J.W., 2001. Uncertainty in source partitioning using stable isotopes.
859 Oecologia 127, 171-179. https://doi.org/10.1007/s004420000578.

860 62 Rau, G. H., Riebesell, U., Wolf-Gladrow, D., 1996. A model of photosynthetic C-13
861 fractionation by marine phytoplankton based on diffusive molecular CO_2 uptake. Mar. Ecol. Prog.
862 Ser. 133, 275–285.Rebello, A. L., Ponciano, C. R., Melges, L. H. 1988. Avaliação da

produtividade primaria e da disponibilidade de nutrientes na Baia de Guanabara. An. Acad. Bras. Cienc., 60, 419–430.

63 Ribeiro, C., Kjerfve, B., 2002. Anthropogenic influence on the water quality in Guanabara Bay, Rio de Janeiro, Brazil. Reg. Environ. Chang. 3, 13–19. http://dx.doi.org/10.1007/s10113-001-0037-5.

64 Robbins, L. L., Hansen, M. E., Kleypas, J. A., Meylan. S. C., 2010. CO2 Calc: a user-friendly seawater carbon calculator for Windows, Max OS X, and iOS (iPhone), U.S. Geological Survey Open-File Report, 2010–1280, 1–17, available at: http://pubs. usgs.gov/of/2010/1280/.

65 Samanta, S., Dalai, T. K., Pattanaik, J. K., Rai, S. K., Mazumdar, A., 2015. Dissolved inorganic carbon (DIC) and its $\delta^{13}C$ in the Ganga (Hooghly) River estuary, India: Evidence of DIC generation via organic carbon degradation and carbonate dissolution. Geochim. Cosmochim. Acta, 165, 226–248. https://doi.org/10.1016/j.gca.2015.05.040.

66 Siegenthaler, U. and K. O. Miinnich. 13C/12C fractionation during CO2 transfer from air to sea. In Bolin, B., editor, SCOPE 16 - The Global Carbon Cycle, pages 249-257. Wiley & Sons, New York, 1981.

67 Strickland, J. D. H., Parsons, T. R., 1972. A practical handbook of seawater analysis, 2nd ed. Fisheries Research Board of Canada Bulletin.

68 Van Dam, B. R., Tobias, C., Holbach, A., Paerl, H. W. Zhu, G., 2018. CO2limited conditions favor cyanobacteria in a hypereutrophic lake: An empirical and theoretical stable isotope study. Limnol. Oceanogr. 63, 1643–1659. https://doi.org/10.1002/lno.10798.

69 Wang, X., Luo, C., Ge, T. Xu, C. Xue, Y., 2016. Controls on the sources and cycling of dissolved inorganic carbon in the Changjiang and Huanghe River estuaries, China: ^{14}C and ^{13}C studies. Limnol. Oceanogr. 61(4), 1358–1374. https://doi.org/10.1002/lno.10301

70 Yang X., Xue, L., Li, Y., Han, P., Liu, X., Zhang, L., Cai, W.-J., 2018. Treated Wastewater Changes the Export of Dissolved Inorganic Carbon and Its Isotopic Composition and Leads to Acidification in Coastal Oceans. Environ. Sci. Technol. 52, 5590–5599. https://doi.org/10.1021/acs.est.8b00273.

71 Zeebe, R. E., Wolf-Gladrow, D., 2001. CO_2 in Seawater: Equilibrium, Kinetics, Isotopes. Elsevier Oceanography Series, 65Amsterdam.

72 Zhang, J., P. D. Quay, and D. O. Wilbur (1995), Carbon isotope fractionation during gas-water exchange and dissolution of CO_2, Geochim. Cosmochim. Acta, 59(1), 107–114, doi:10.1016/0016-7037(95)91550-D.

Graphical Abstract